ORIGINAL PAPER

Periodic solutions of nonlinear delay differential equations using spectral element method

**Firas A. Khasawneh · David A.W. Barton ·
Brian P. Mann**

Abstract We extend the temporal spectral element method further to study the periodic orbits of general autonomous nonlinear delay differential equations (DDEs) with one constant delay. Although we describe the approach for one delay to keep the presentation clear, the extension to multiple delays is straightforward. We also show the underlying similarities between this method and the method of collocation. The spectral element method that we present here can be used to find both the periodic orbit and its stability. This is demonstrated with a variety of different examples, namely, the delayed versions of Mackey–Glass equation, Van der Pol equation, and Duffing equation. For each example, we show the method's convergence behavior using both p and h refinement and we provide comparisons between equal size meshes that have different distributions.

F.A. Khasawneh (✉) · B.P. Mann
Department of Mechanical Engineering and Materials Science, Duke University, Durham, NC 27708, USA
e-mail: firas.khasawneh@duke.edu

D.A.W. Barton
Department of Engineering Mathematics, University of Bristol, Bristol, BS8 1TR, UK

Delay differential equations (DDEs) have been successfully used to model many different phenomena occurring in science and engineering contexts. Specific areas in which DDEs have been used extensively include machining dynamics [7, 10, 40], systems biology [2, 8, 34] and laser systems [26, 37]. In some models, for example in systems biology related applications, delays are used to avoid modeling certain processes that are known to take a predetermined amount of time but otherwise contribute little to the dynamics. In other models, for example in machining dynamics, the delay is intrinsic to the system and cannot be removed.

DDEs are infinite dimensional dynamic systems whose state-space is typically taken to be the space of continuous functions. Therefore, DDEs require a function segment over a period of time as an initial condition rather than a point value at time zero as with an ordinary differential equation. The infinite dimensionality of DDEs significantly complicates the resulting analysis from both an analytical and numerical perspective [20, 39]. Furthermore, complicated behavior can be readily observed in seemingly low-order equations [4, 21].

Due to the difficulties associated with the analytical aspects of DDEs, there has been significant focus on their numerical solution. The majority of this work has focused on initial value solvers, mostly extending Runge–Kutta solvers to DDEs [5, 16, 18]. Alternatively, other solvers based on an implicit Radau method, e.g., RADAR5 by Guglielmi and Hairer [17],

have also been used to solve stiff DDEs. These solvers were designed to handle the specific complexities of DDEs, such as the propagation of discontinuities caused by the initial conditions. In this study, however, we are interested in long-time dynamics, namely periodic orbits. The numerical methods for analyzing periodic orbits directly as boundary value problems are much less developed than the corresponding methods for initial value problems. These methods typically use a collocation-type discretization based on Chebyshev or Gauss–Legendre points [3, 13, 14, 28]. Stability of the periodic orbit may then be derived from the linearization of the discretized system.

In this study, we consider an alternative approach to numerically approximating periodic orbits of nonlinear DDEs based on the temporal spectral element method, which is a type of (piecewise) Galerkin method [24]. The temporal spectral element method for delay systems is a modification of the spatial spectral element method which has been widely used in simulating the partial differential equations arising in models of fluids and structures [33, 41]. The temporal spectral element method can also be viewed as an evolution of the state-space temporal finite element method (state-space TFEA) which has been used to study the stability of equilibria of linear DDEs [25, 31, 38]. We also show the underlying similarities between this method and the method of collocation.

With the spectral element method, we seek to study the periodic orbits of general nonlinear DDEs of the form

$$\frac{\mathrm{d}x}{\mathrm{d}t} = g\big(x(t), x(t-\tau)\big), \tag{1}$$

with one constant delay $\tau > 0$, and $g : \mathbb{R}^n \times \mathbb{R}^n \to \mathbb{R}^n$ is a continuously differentiable function. Although we describe the approach for one delay to keep the presentation clear, the extension to multiple delays is straightforward. The spectral element method that we present here can be used to find both the periodic orbit and its stability. This is demonstrated with a variety of different examples; specifically, we study the periodic orbits of the delayed Mackey–Glass equation, the delayed Van der Pol equation and the delayed Duffing equation.

The organization of this paper is as follows. Section 1 describes the formulation of the boundary value problem (BVP) used to solve for the periodic orbits. Section 2 describes the discretization method used to

obtain a finite dimensional approximation of the infinite dimensional DDE. Section 3 describes a solution method based on the spectral element approach to obtain periodic orbits of (1). Section 4 describes obtaining the linearized stability of the periodic orbit using the Floquet theory. Section 5 provides several case studies to demonstrate the effectiveness of the current approach while Sect. 6 contains concluding remarks.

1 Problem formulation

The periodic orbits of (1) can be obtained as the solutions of an infinite dimensional boundary value problem (BVP). This BVP has three components:

1. The equation describing the system evolution with time (e.g., see (1)).
2. The periodicity condition $x(s) = x(s + T)$ for $s \in [-\tau, 0]$.
3. A phase condition which removes any translational invariance in the system and so ensures a unique solution to the BVP.

These three components are discussed in more detail in Sects. 1.1, 1.2, and 1.3.

Since it is not possible to deal directly with the infinite dimensional BVP numerically, it must first be discretized to produce a finite dimensional approximation. The idea is that as the degree of approximation increases, the solution of the finite dimensional problem converges to that of the infinite dimensional problem.

General convergence proofs for different discretizations and solution methods are very sparse in the current literature and typically focus on collocation as the solution method, e.g., [13]. In the collocation method, the evolution equation (1) is required to hold exactly at finitely many collocation points. The spectral element method described here instead uses weighted integrals across the temporal domain. Nevertheless, there is a connection between collocation methods and the spectral element approach as will be shown in Sect. 3.

Regardless of the discretization method (Sect. 2) or the solution method (Sect. 3), the end result is a large system of algebraic equations which must then be solved using a general nonlinear root finding method, e.g., a Newton iteration. One additional benefit to using a Newton iteration is that stability information (Floquet multipliers) of the periodic orbit can be determined from the Jacobian used in the last step of the iteration.

1.1 The evolution equation

As previously described, any periodic solution of (1) can be found by solving a related two-point BVP. Since, in general, the period of the orbit is an additional unknown, time is rescaled such that $t = T\tilde{t}$; thus, the true period enters into the equations as an explicit variable T and the time period over which the BVP is posed becomes simply unity. After dropping tildes and rearranging, the equation describing the evolution of the DDE for $t > 0$ becomes

$$f = \frac{dx}{dt} - Tg\big(x(t), x(t - \tau/T)\big) = 0, \quad t \in [0, 1],$$

(2)

where g is twice continuously differentiable and T is the unknown period of the orbit.

1.2 The periodicity condition

The second component of the two-point BVP is the periodicity condition which requires that the states at $t - \tau/T < 0$ be mapped back to [0, 1]. This condition can be described by

$$x(s) = x(s + 1), \quad s \in [-\tau/T, 0].$$

(3)

In this study, we use the modulo operator for $t - \tau/T < 0$ combined with algebraic equations at $t = 0$—whose number is equal to the number of states—to enforce the periodicity condition; see Sect. 3.

1.3 The phase condition

There are several possible choices for the phase condition, for example, fixing one of the solution components at $t = 0$ [36]. Another choice is to use a discrete orthogonality condition $(x(0) - x_0(0))^T \dot{x}_0(0) = 0$, where x_0 is the initial solution and x is the corrected solution. However, the most commonly used alternative is to impose the functional orthogonality relationship

$$p(x) = \int_0^1 x_0^T(t)\dot{x}(t)\,dt,$$

(4)

where $\dot{x} := \frac{dx}{dt}$ and the superscript "T" denotes the matrix transpose [12]. This condition minimizes the difference between $x_0(t)$ (the initial guess) and $x(t)$ with respect to translation.

Combining (2)–(4), the two-point BVP can be written as

$$\begin{cases} f = \frac{dx}{dt} - Tg(x(t), x(t - \tau/T)) = 0, \\ \quad t \in [0, 1] \text{ (evolution)}, \\ x(s) - x(s + 1) = 0, \\ \quad s \in [-\tau/T, 0] \text{ (periodicity)}, \\ p(x) = 0 \quad \text{(phase)}. \end{cases}$$

(5)

2 Discretization method

There are several methods to discretize the periodic orbits of (5); they are mostly polynomial approximations of the form

$$x(t) = \sum_{i=1}^{n+1} x_i \phi_i(t),$$

(6)

where $t_i \in [0, 1]$ is the set of discretization points, $x_i = x(t_i)$, and ϕ_i are the basis or trial function which can be defined globally or piecewise. These methods are distinguished by (1) the location of the discretization points, and (2) the method for minimizing the residual error [9, 35]. The location of the discretization points determines the approximation interpolant and its derivatives.

The choice of the discretization mesh, and hence the approximation basis, is also dependent on the method used for minimizing the residual error. For example, if a Galerkin type approach is used, the selected mesh needs to accommodate an accurate quadrature rule such as a Gaussian quadrature. For collocation type methods, the mesh nodes need to be optimally placed to guarantee minimal residual error, e.g., the nodes coincide with the roots or extrema of orthogonal polynomials.

Examples of common discretization nodes include the roots or the extrema of Chebyshev, Legendre, or Hermite polynomials. Each of these meshes yields a well-conditioned system, minimizes the residual error and accommodates accurate Gauss quadrature rules. Consequently, any of these meshes can be used in solutions that are based on collocation or Galerkin methods. Alternatively, a Fourier approach can also be used to find the periodic solution.

A Fourier approach has the advantage of automatically incorporating a periodicity assumption which eliminates the need for adding a periodicity condition.

However, the Fourier approach cannot be used for stability calculations; hence, additional steps are necessary to determine the stability of the DDE [9].

In this study, we use a piecewise polynomial approximation. The time interval [0, 1] is discretized into a finite number of temporal elements E. Each element is described by the interval

$$e_j = [t_j^-, t_j^+),\qquad(7)$$

where j is the element index while t_j^- and t_j^+ denote the left and right element boundaries, respectively, with the length of the jth element given by

$$h_j = t_j^+ - t_j^-.\qquad(8)$$

A polynomial approximation is then used to obtain an approximate expression for the states over each element. For example, the states over the jth element are approximated by

$$x_j(t) = \sum_{i=1}^{n+1} \phi_i(\eta) x_{ji},\qquad(9)$$

where n is the order of the interpolating polynomial, $\eta \in [0, 1]$ is the local time in the element normalized by the length of the element, while $x_{ji} = x_j(t_i)$ is the state vector at the ith interpolation node within the jth element.

Lagrange interpolation can be used to obtain the trial functions according to

$$\phi_i(\eta) = \frac{\prod_{k=1,k\neq i}^{n+1}(\eta - \eta_k)}{\prod_{k=1,k\neq i}^{n+1}(\eta_i - \eta_k)},\qquad(10)$$

where the indices i and k refer to the ith and kth interpolation nodes, respectively. The Lagrange polynomial ϕ_i corresponding to the ith node has the property

$$\phi_i(\eta_k) = \begin{cases} 1, & i = k, \\ 0, & \text{otherwise}, \end{cases} \quad j, k = 1, \dots, n+1.\qquad(11)$$

Equation (10) comes from the typical form of Lagrange interpolation which is only recommended for a small number of nodes. Specifically, using this equation with high values for n requires a high number of additions and multiplications and yields the computation numerically unstable [6]. A more effective representation of Lagrange polynomials is provided by the barycentric formula according to [22]

$$\phi_i(\eta) = \frac{\frac{\varpi_i}{\eta - \eta_i}}{\sum_{k=1}^{n+1} \frac{\varpi_k}{\eta - \eta_k}},\qquad(12)$$

where ϖ_k are the barycentric weights given by

$$\varpi_k = \frac{1}{\prod_{k\neq j}(\eta_j - \eta_k)}, \quad j = 1, \dots, n+1.\qquad(13)$$

The barycentric formula requires less computational effort and has better numerical stability than the conventional Lagrange representation [6, 22]; therefore, it is used to generate the trial functions in the present study.

Equation (12) can also be used to define an interpolation matrix that maps a set of arbitrary but distinct points onto the set of interpolation points (also called the base points). For example, let the vector of base points be $x_1 \in \mathbb{R}^{n \times 1}$, and let the vector of the arbitrary unique points be $x_2 \in \mathbb{R}^{m \times 1}$, then the effect of interpolating x_2 using x_1 as the base points is described using the linear transformation

$$x_2 = \Upsilon x_1,\qquad(14)$$

where $\Upsilon \in \mathbb{R}^{m \times n}$ is called the interpolation matrix. The entries of the interpolation matrix are calculated using (12) according to

$$\Upsilon_{ji} = \phi_i(\eta_j),\qquad(15)$$

where $\eta_j \in x_2$ and $i \in 1, 2, \dots, n$. Equations (14) and (15) define a linear transformation useful in interpolating the delayed states in terms of the discretization nodes.

In addition to being a more efficient tool to generate the trial functions, the barycentric weights can be used to obtain the value of the derivative of the trial functions evaluated at the interpolation nodes according to

$$\phi_i'(\eta_k) = \begin{cases} \frac{\varpi_i/\varpi_k}{\eta_i - \eta_k}, & i \neq k, \\ \sum_{i=0,i\neq k}^{n+1} \frac{-\varpi_i/\varpi_k}{\eta_i - \eta_k}, & i = k. \end{cases}\qquad(16)$$

These values are useful in evaluating the weighted residual integrals in Galerkin-type methods using a Gauss quadrature. Moreover, the values defined in (16) form the entries of the differentiation matrix which describes a linear transformation from the values of the

trial functions at the nodes to the values of the derivative of the trial functions at the same nodes. For example, assume that the vector $z \in \mathbb{R}^{n+1}$ contains the values of a function $G(t) : [0, \infty) \to \mathbb{R}$ evaluated at the $n+1$ interpolation points. If the vector z' contains the derivative of G evaluated at the same collocation points, then the effect of differentiating the function at these points can be described by a differentiation matrix $D \in \mathbb{R}^{n+1 \times n+1}$ according to

$$z' = D z, \tag{17}$$

where the entries of D are defined from (16) according to

$$D_{ki} = \phi_i'(\eta_k). \tag{18}$$

In this study we use the Legendre–Gauss–Lobatto points (LGL) as the interpolation nodes within each elements. These points are obtained from solving for the roots of the equation

$$\left(1 - u^2\right) L_n'(u) = 0, \tag{19}$$

where u ranges from -1 to 1 and $L_n(u)$ is the Legendre polynomial of order n [41]. These points can be shifted to an arbitrary interval $[a, b]$ through the relation

$$\tilde{u} = \frac{b - a}{2} u + \frac{b + a}{2}, \tag{20}$$

where $u \in [-1, 1]$ and $\tilde{u} \in [a, b]$, e.g., if $a = 0$ and $b = 1$, then $\eta = \tilde{u}$. Using the LGL nodes also simplifies the expression for the $(n+1) \times (n+1)$ differentiation matrix in (17) to

$$D_{00} = -D_{nn} = -\frac{n(n+1)}{4}, \tag{21a}$$

$$D_{km} = \begin{cases} \frac{L_n(t_k)}{L_n(t_m)} \frac{1}{(t_k - t_m)}, & k \neq m \\ 0, & \text{otherwise.} \end{cases} \tag{21b}$$

3 Solution method

The periodic solution of (1) is obtained using Newton iteration on the discretized version of the BVP (5). To apply Newton iteration, the discretized version of (5) is written in the form

$$f_u(u) \Delta u = f(u), \tag{22}$$

where $u = \{x_{ji}, T\}$ is the vector of discretized states.

This section derives the expressions that are necessary to apply Newton iteration. Specifically, Sect. 3.1 gives the expression for the residual on the mesh points and the discrete periodicity condition—which are components of the $f(u)$ term in (22). Section 3.2 shows the discrete version of the phase condition while Sect. 3.3 derives the expression $f_u(u)$, which contains the Jacobian used for periodic solution calculations.

3.1 The residual

Substituting (9) into the expression for f in (5) yields the residual on the jth element according to

$$R_j = \sum_{i=1}^{n+1} \frac{1}{h_j} \dot{\phi}_i(\eta) x_{ji}$$

$$- T g \left(\sum_{i=1}^{n+1} \phi_i(\eta) x_{ji}, \sum_{i=1}^{n+1} \phi_i(\eta^*) x_{j^*(t^*),i}^q \right), \tag{23}$$

where the local normalized time is given according to

$$\eta^* = \frac{t^* - t_j^{*-}}{h_j^*}, \tag{24}$$

while the time t^* is defined using modular arithmetics according to

$$t^* = t_j^- + \eta h_j - \tau \pmod 1. \tag{25}$$

The function $j^*(t^*)$ gives the element index to which t^* belongs and it is given by

$$j^*(t^*) = \sum_{j=1}^{E} j \chi_{e_j}(t^*), \tag{26}$$

where the indicator function is defined as

$$\chi_{e_j}(t^*) = \begin{cases} 1 & \text{if } t^* \in e_j, \\ 0 & \text{otherwise.} \end{cases} \tag{27}$$

If the elements are uniformly distributed, then (26) reduces to

$$j^*(t^*) = \left\lceil \frac{t^*}{h} \right\rceil, \tag{28}$$

where $\lceil \cdot \rceil$ is the ceiling function and $h = 1/E$ is the length of each of the uniform elements.

The positive integer q in (23) is the number of the period to which the delay looks back and it is described by the absolute value function

$$q = \left\lVert \left\lfloor \frac{t - \tau}{T} \right\rfloor \right\rVert, \tag{29}$$

where $\lfloor \cdot \rfloor$ is the floor function and with the understanding that $q = 0$ indicates a mapping onto the interval $[0, 1]$.

The values assigned to the index q in (29) are used in the stability analysis which does not make any assumption on the periodicity of the linearized equations; see Sect. 4. However, since in this section, we are seeking a periodic solution of (1), the delayed term is handled using the modulo operation to map the states onto $[0, 1]$ instead of $[-\tau/T, 1]$. Specifically, for obtaining the periodic solution, the substitution $q = 0$ (indicating a mapping onto $[0, 1]$) is made in (23) resulting in the expression

$$R_j = \sum_{i=1}^{n+1} \frac{1}{h_j} \dot{\phi}_i(\eta) x_{ji}$$
$$- Tg \left(\sum_{i=1}^{n+1} \phi_i(\eta) x_{ji}, \sum_{i=1}^{n+1} \phi_i(\eta^*) x_{j^*(t^*),i} \right), \tag{30}$$

where $q = 0$ was omitted to simplify notation. This substitution eliminates the unknowns corresponding to $t < 0$ and implicitly enforces the periodicity condition for $t < 0$. Nevertheless, the periodicity condition at $t = 0$ still needs to be enforced explicitly according to

$$x(0) - x(1) = 0, \tag{31}$$

where for a d-dimensional system, (31) gives d equations.

Using the method of weighted residuals on (23) results in

$$\int_0^1 \left(\sum_{i=1}^{n+1} \frac{1}{h_j} \dot{\phi}_i(\eta) x_{ji} - Tg \right) \psi_p(\eta) \, d\eta = 0, \tag{32}$$

where ψ_p are weight functions with $p \in \{1, 2, \ldots, n\}$. A discrete version of the integral in (32) can be obtained using Gaussian quadrature rules. To illustrate, recall that a Legendre–Gauss–Lobatto (LGL) quadra-ture rule can be used to approximate integrals according to

$$\int_a^b F(t) \, dt \approx \frac{b - a}{2} \sum_{k=1}^{m+1} w_k F(t_k), \tag{33}$$

where t_k and w_k are the LGL quadrature nodes and weights, respectively. In this study, we chose the quadrature nodes to be identical to the interpolation nodes whereas the quadrature weights were calculated using [32]

$$w_k = \begin{cases} \frac{2}{n(n+1)}, & k = 1, n+1, \\ \frac{2}{n(n+1)(L_n(\eta_k))^2}, & \text{otherwise.} \end{cases} \tag{34}$$

If $F(\eta)$ is a polynomial with a degree of at most $2n + 1$, then it is sufficient to use $n + 1$ points in the Gauss quadrature to yield an exact estimate of the integral [15].

Using an LGL quadrature in (32) results in

$$\sum_{k=1}^{n+1} \left(\sum_{i=1}^{n+1} \frac{1}{h_j} \dot{\phi}_i(\eta_k) x_{ji} - Tg \right) \psi_p(\eta_k) \, w_k = 0. \tag{35}$$

Let the value of the initial guess of the states on the interpolation points within the jth element be represented by the vector $\mathbf{x}_0$. The delayed states $\mathbf{x}_\tau$ are then obtained using interpolation according to

$$\mathbf{x}_\tau = \Upsilon_{(t^* \to t)} \mathbf{x}_0, \tag{36}$$

where Υ is the matrix that interpolates the delayed states in terms of the states at the interpolation points, see (15). In addition, let $\hat{D}_j$ be the differentiation matrix on the jth element obtained using the Kronecker product

$$\hat{D}_j = \frac{1}{h_j} D \otimes I_d, \tag{37}$$

where D is given by (21) while I_d is the $d \times d$ identity matrix and d is the order of the nonlinear DDE. Using the above definitions, (35) can be written as

$$R = \mathbf{W}_{\text{res}} \hat{R} = 0, \tag{38}$$

where $\hat{R}$ is given by

$$\hat{R} = \hat{D} \mathbf{x}_0 - Tg(\mathbf{x}_0, \Upsilon_{(t^* \to t)} \mathbf{x}_0), \tag{39}$$

while the $d(En + 1) \times d(En + 1)$ matrix $\hat{D}$ is the global differentiation matrix which contains all the individual element differentiation matrices $\hat{D}_j$. The matrix $\mathbf{W}_{\text{res}} : \mathbb{R}^{d(En+1)} \to \mathbb{R}^{dEn}$ is given by

$$
\mathbf{W}_{\text{res}} = \left(\begin{bmatrix} w_0 & w_1 & \dots & w_n \\ w_0 & w_1 & \dots & w_n \\ \vdots & \vdots & \ddots & \vdots \\ w_0 & w_1 & \dots & w_n \end{bmatrix} \right.
$$
$$
\left. \circledast \begin{bmatrix} \psi_0(t_0) & \dots & \psi_0(t_n) \\ \psi_1(t_0) & \dots & \psi_1(t_n) \\ \vdots & \ddots & \vdots \\ \psi_{n-1}(t_0) & \dots & \psi_{n-1}(t_n) \end{bmatrix} \right) \otimes \mathbf{I}_q,
$$
$$(40)$$

where w_k are the interpolation weights given by (34) while the symbol $\circledast$ denotes element-wise multiplication.

Convergence can then be obtained by increasing the number of elements E and/or the order of the interpolation polynomial n. The method described above which uses weighted residual integral to minimize the error and uses quadratures to approximate integrals is called the spectral element method [9]. This method allows hp-refinement schemes and can yield higher rates of convergence (spectral rates of convergence). It is interesting to point out the connection between the spectral element method we present here and the typical collocation methods. This connection is best described using (38) and (39). In fact, the term $\hat{R}$ in (38) is similar to the matrices that are generated from a collocation scheme—where a set of algebraic equations is produced by evaluating the DDE at the collocation points. The effect of invoking the spectral element method is therefore described by (39) and it can be thought of as a linear transformation of $\hat{R}$.

Note that the discretization of f in (5) using E elements and $n + 1$ interpolation nodes gives rise to $d(En + 1)$ unknown states. Appending the unknown period T as the last entry in the vector of states $u = \{x_{ji}, T\}$ further increases the number of unknowns to $d(En + 1) + 1$. To solve for the unknowns it is necessary to obtain at least an equal number of equations.

Equation (38) provides dEn equations while the periodicity condition in (31) provides d more equations. The last additional equation, corresponding to the phase condition, is set to zero. Setting this entry

to zero is equivalent to stating that the phase condition is always satisfied. The specific phase condition described in (4) is taken into account in the term $f_u(u)$ of (22) as will be shown in Sect. 3.3. Consequently, $d(En + 1) + 1$ equations are obtained to solve for the equal number of unknowns and they are arranged into the column vector

$$
f(u) = \begin{bmatrix} R \\ x(0) - x(1) \\ 0 \end{bmatrix}. \tag{41}
$$

Equation (41) provides the expression for one of the components in (22) that are necessary to apply Newton iteration. The other components are described in the following sections.

3.2 Discretized phase condition

Recall that the phase condition is necessary to ensure a unique solution to (5). Assume that the order of the DDE is d and that the interval $[0, 1]$ was divided into E elements each with $n + 1$ interpolation nodes. The phase condition in (4) can be described piecewise over all the elements covering $[0, 1]$ according to

$$
p(x) = \int_0^1 \dot{x}_0^{\mathrm{T}} x \, dx = \sum_{j=1}^{E} \int_{t_j^-}^{t_j^+} \dot{x}_0^{\mathrm{T}} x \, dx. \tag{42}
$$

If a quadrature rule is defined on the $n + 1$ base nodes within each element, (42) can be approximated by

$$
p(x) \approx \sum_{j=1}^{E} \frac{h_j}{2} \sum_{k=1}^{n+1} w_k \dot{x}_{0k} x_{jk}, \tag{43}
$$

where w_k are the quadrature weights.

Let $\mathbf{x}_0 \in \mathbf{R}^{d(En+1)}$ contain the initial guess of the states on the base points. Further, let $\mathbf{x} \in \mathbb{R}^{d(En+1)}$ contain the true states on the same mesh.

Choosing the quadrature points to be identical to the discretization points on $[0, 1]$, the discretized phase condition reads

$$
p(\mathbf{x}) = \left(\hat{D} \mathbf{x}_0 \right)^{\mathrm{T}} \circledast (\mathbf{w} \otimes \mathbf{1}_{1 \times d}) \mathbf{x}, \tag{44}
$$

where $\circledast$ indicates element-wise multiplication, $\mathbf{1}_{1 \times d}$ is a $1 \times d$ vector of ones while the $1 \times (En + 1)$ vector $\mathbf{w}$ is given by

$$
\mathbf{w} = \begin{bmatrix} \dfrac{h_1 w_1}{2} & \dfrac{h_1 w_2}{2} & \dots & \dfrac{h_1 w_{n+1} + h_2 w_1}{2} & \dots \\[2ex] & \dfrac{h_E w_1}{2} & \dfrac{h_E w_2}{2} & \dots & \dfrac{h_E w_{n+1}}{2} \end{bmatrix}. \tag{45}
$$

Note that in **w** the entries at the beginning and end of any two subsequent elements are added together.

3.3 The Jacobian

The other necessary component to apply Newton iteration on (30) is the term $f_u(u)$. This term contains the linearized version of (30). The linearization of (30) can be written in the form $f_u(u)\Delta u = f(u)$ according to

$$
\begin{aligned}
\sum_{i=1}^{n+1} &\dot{\phi}_i(\eta)\Delta x_{ji} - TA_0(\alpha)\sum_{i=1}^{n+1}\phi_i(\eta)\Delta x_{ji} \\
&- TA_1(\alpha)\sum_{i=1}^{n+1}\dot{\phi}_i(\eta^*)\Delta x_{j^*,i} - g(\alpha)\Delta T \\
&- \frac{\tau}{T}A_1(\alpha)\sum_{i=1}^{n+1}\dot{\phi}_i(\eta^*)x_{j^*,i}\Delta T \\
&= -\sum_{i=1}^{n+1}\dot{\phi}_i(\eta)x_{ji} + Tg(\alpha),
\end{aligned}
\tag{46}
$$

where

$$
\alpha = \left(\sum_{i=1}^{n+1}\phi_i(\eta)x_{ji}, \sum_{i=1}^{n+1}\phi_i(\eta^*)x_{j^*,i}\right)
$$

and

$$
A_0(\zeta,\eta) = \frac{\partial}{\partial\zeta}g(\zeta,\eta),
\tag{47a}
$$

$$
A_1(\zeta,\eta) = \frac{\partial}{\partial\eta}g(\zeta,\eta).
\tag{47b}
$$

Evaluating (46) on the $(En+1)$ mesh points and arranging the terms into matrices results in

$$
J\begin{bmatrix}\Delta\mathbf{x}\\\Delta T\end{bmatrix} = -\hat{R},
\tag{48}
$$

where $\Delta\mathbf{x} = \mathbf{x} - \mathbf{x}_0$, $\hat{R}$ was described in (39) and the matrix J has the dimensions $d(En+1) \times d(En+1) + 1$.

The spectral element method is applied by multiplying both sides of (48) by $\mathbf{W}_{\text{res}}$ according to

$$
\mathbf{W}_{\text{res}}J\begin{bmatrix}\Delta\mathbf{x}\\\Delta T\end{bmatrix} = -\mathbf{W}_{\text{res}}\hat{R}.
\tag{49}
$$

Define the $dEn \times d(En+1) + 1$ matrix $\hat{J}$ as $\hat{J} = \mathbf{W}_{\text{res}}J$. The term $f_u(u)$ in (22) is then obtained by appending the continuity condition at $t = 0$ (i.e., $x^1(1) = x^0(0)$) and the phase condition (44) to $\hat{J}$. Specifically, the expression for $f_u(u)$ is given by

$$
f_u(u) = \begin{bmatrix} & & \hat{J} & & & \\ \mathbf{I}_d & \mathbf{0}_d & \dots & \mathbf{0}_d & -\mathbf{I}_d & 0 \\ & & p(\mathbf{x}) & & & 0 \end{bmatrix},
\tag{50}
$$

where $p(\mathbf{x})$ is given by (44). Equations (50) and (41) can then be used in a Newton iteration algorithm (see (22)) to solve for the states on the mesh points as well as the period of the orbit.

4 Stability calculations

The basic tools to analyze the local stability of the periodic orbits of (1) are the monodromy matrix and Floquet theory. The monodromy matrix Q is the discretization of the time integration operator of the linearized equation [28]. The discretization is performed without the modulo operation, i.e., the linearized equation is discretized on $[-\bar{\tau}/T, 1]$. This corresponds to the linearization described in (23) except the index q is maintained to keep track of the periods the delay looks back to.

The linearized equations for stability analysis will have a form similar to (46) with two main differences: (1) the substitution $x_{j^*,i} = x_{j^*,i}^q$ is made to ensure correct mapping and (2) the partial derivatives with respect to T are omitted. The monodromy matrix represents a linear map from the states in the segment $[-\tau/T, 0]$ onto the states in the segment $[-\tau/T + 1, 1]$ according to

$$
u_T = Qu_0,
\tag{51}
$$

where $u_T \in [-\bar{\tau}/T + 1, 1]$ and $u_0 \in [-\bar{\tau}/T, 0]$. The stability of the periodic solutions is found from calculating the eigenvalues (Floquet multipliers) of the monodromy matrix. Besides a trivial $+1$ Floquet multiplier for autonomous systems, the system is stable if the remaining multipliers are within the unit circle in the complex plane; see Fig. 1. The computed eigenvalues of Q form approximations to the eigenvalues of the integration operator.
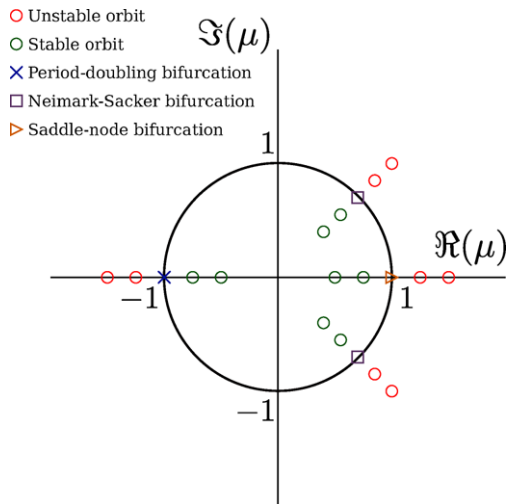
Fig. 1 The stability criteria dictates that all the eigenvalues μ of the monodromy operator Q should lie within the unit circle in the complex plane. Moreover, the manner in which the eigenvalues depart the unit circle produces different bifurcation behavior as shown

As the discretization is refined by increasing the number of the LGL nodes, and, consequently, the order of the trial functions, more Floquet multipliers are better approximated.

5 Examples

To demonstrate the effectiveness of the current approach, we calculate the periodic orbits and their stability for several case studies. We also calculate the errors associated with the approximate periodic orbits using the error norms described in Sect. 5.1. Section 5.2 studies the Mackey–Glass equation. Sections 5.3 and 5.4 study the delayed Van der Pol equation and the delayed Duffing equation, respectively. In each case, the periodic orbit is calculated and plotted and its stability is ascertained using the procedure described in Sect. 4.

5.1 Error analysis

This section describes the error norms used in this study. The error is calculated between the spectral element solution and a reference solution for different mesh sizes. This then enables the calculation of the rate of convergence of the spectral element solution.

The norms typically used to quantify the error can be categorized into continuous and discrete norms. Continuous norms are defined over the whole period whereas discrete norms are only defined at the representation points. However, although discrete norms show the super-convergence effects more clearly, they do not always provide a good indication of the quality of the overall solution [3]. The two most common norms are the L_2 and the L_∞ norms defined as

$$\|x\|_2 = \left(\int_0^1 \left(x(t) - \tilde{x}(t) \right)^2 \mathrm{d}t \right)^{\frac{1}{2}} \quad (L_2 \text{ norm}), \quad (52a)$$

$$\|x\|_\infty = \max_{t \in [0,1]} \left(x(t) - \tilde{x}(t) \right) \quad (L_\infty \text{ norm}), \quad (52b)$$

$$\|x\|_2 = \left(\sum_{k=1}^{n+1} (x_k - \tilde{x}_k)^2 \right)^{\frac{1}{2}} \quad (\ell_2 \text{ norm}), \quad (52c)$$

$$\|x\|_\infty = \max_k |x_k - \tilde{x}_k| \quad (\ell_\infty \text{ norm}), \quad (52d)$$

where $\tilde{x}$ is the reference solution, upper-case L denotes a continuous norm while lower-case ℓ denotes a discrete norm. Because of its extensive use in other numerical continuation packages such as AUTO [11], we will use the L_2 norm in this study. Further, the discrete norms ℓ_2 and ℓ_∞ will also be used to get a better idea about the errors.

Equations (52) makes use of a reference solution $\tilde{x}$ which ideally would be an exact analytical solution. In general, exact solutions of DDEs are not known and instead a high accuracy solution using an approximation technique is used. The steps used in refining the mesh and calculating the error are as follows:

1. Generate a high precision solution $\tilde{x}$, e.g., using 1,000 mesh points.
2. Generate the lower resolution initial solution x_{ini} from $\tilde{x}$ using interpolation. This is the initial solution that is used in the next step. Generating the initial guess for the coarse solution from the reference solution ensures that there is no phase shift between the two solutions.
3. Refine the initial solution x_{ini} from the previous step using spectral element approach to obtain the lower resolution solution x.
4. Use the selected norm from (52) to calculate the error between x and $\tilde{x}$.
5. Increase the resolution and repeat the above steps to calculate the error for various meshes.

Fig. 2 The periodic solution and the error norms for (53) (where $T \approx 20.08$). The reference solution was obtained using $n = 1,000$ and $E = 1$ while the error norms were calculated using (52a), (52c), and (52d). In the error plots, the values $E = 1, 2, 3$ were used whereas n was varied in the range $2 \leq n \leq 50$
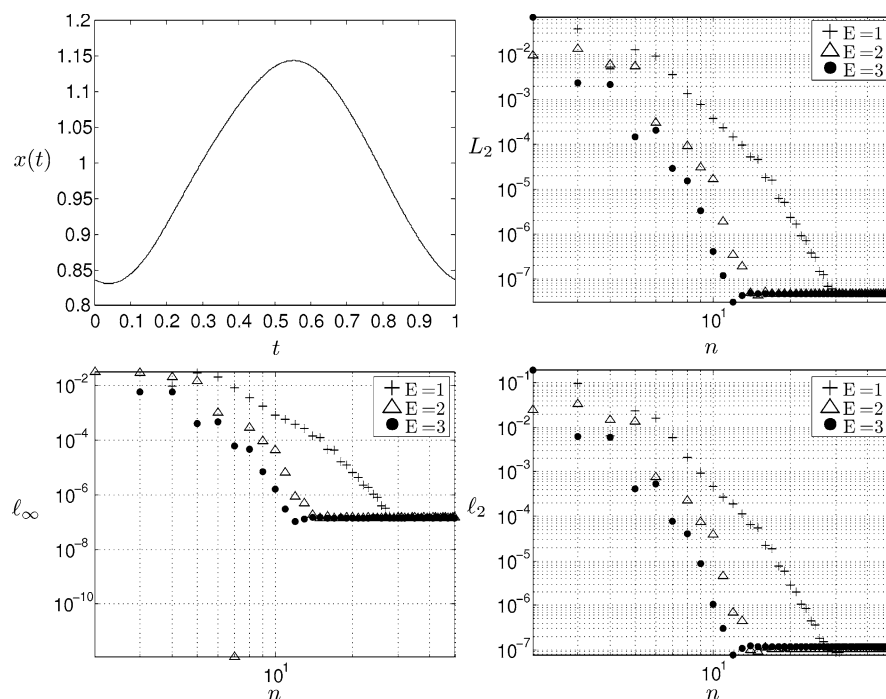
5.2 Mackey–Glass equation

The Mackey–Glass equation models the regeneration of white blood cells [19, 29]. It is one of the classical examples for using nonlinear DDEs in characterizing physiological phenomena. The Mackey–Glass equation is given by

$$\frac{\mathrm{d}}{\mathrm{d}t} x(t) = ax(t) + b \frac{x(t - \tau)}{1 + x^c(t - \tau)}, \tag{53}$$

where a, b, and c are scalars. For $a = 1$, $b = 1.5$, $c = 10$, and $\tau = 2$, there is a stable periodic solution, shown in Fig. 2, with period $T \approx 20.08$.

The results of the error analysis associated with using the spectral element method are also shown in Fig. 2. The reference solution shown in these figures was obtained using the spectral element method with $n = 1,000$ and $E = 1$ and it matched the solution obtained from numerical simulation. For each error norm, three curves corresponding to $E \in \{1, 2, 3\}$ are plotted as a function of n where $2 \leq n \leq 50$. For each value of E and n, an initial solution was constructed from the reference solution to eliminate phase shifts between the reference solution and the final solution. The initial solution was then refined using Newton iteration. It can be seen that the method converges exponentially as evidenced by all the considered error norms. For each error norm, there is a saturation point where the error is no longer decreased with increasing n and E indicating a close match with the reference solution. Using the stability analysis described in Sect. 4, the periodic orbit was found to be stable.

Note that in Fig. 2 the convergence rate improved by increasing the number of elements, and consequently the number of the mesh points. However, with the spectral element method there are two techniques that can be used to increase the size of the mesh: (1) fix the number of elements and increase the order of the interpolation polynomial (*p*-refinement) and (2) fix the order of the polynomial and increase the number of elements (*h*-refinement). Whereas the former technique was investigated in Fig. 2, the latter technique was studied in Fig. 7.

In Fig. 7, the L_2 norm is plotted against the length of the uniform elements $h = 1/E$. The L_2 norm was chosen in this figure since it describes the quality of the overall solution. The order of the interpolation polynomial was held constant at either 3, 4, or 5 while the length of the uniform elements was varied between $1/500 \leq h \leq 1$, i.e., $1 \leq E \leq 500$. Figure 7a shows the plot that corresponds to the L_2 error norm of (53). It is shown that as n was held constant and h was decreased, the error norm decreased linearly until it reached a saturation point where any further re-

Table 1 A comparison of the error values for (53) using different combinations of E and n that yield meshes with the same number of points

E = 1				E = 2				E = 3			
n	L_2	ℓ_2	ℓ_∞	n	L_2	ℓ_2	ℓ_∞	n	L_2	ℓ_2	ℓ_∞
18	$6.23e-6$	$7.69e-6$	$1.55e-5$	9	$3.05e-5$	$7.41e-5$	$9.24e-5$	6	$2.02e-4$	$5.43e-4$	$4.57e-4$
24	$3.66e-7$	$4.48e-7$	$1.05e-6$	12	$3.43e-7$	$6.84e-7$	$8.53e-7$	8	$1.54e-5$	$4.15e-5$	$4.50e-5$
30	$5.09e-8$	$8.77e-8$	$1.44e-7$	15	$4.19e-8$	$9.26e-8$	$1.40e-7$	10	$4.09e-7$	$1.07e-6$	$1.57e-6$
36	0	0	0	18	$4.65e-8$	$1.06e-7$	$1.41e-7$	12	$3.07e-8$	$7.88e-8$	$1.04e-7$

duction in the element length did not influence convergence. From the numerical data in Table 4, the *h*-refinement rate of convergence for (53) was approximately $O(h^n)$, where n is the order of the interpolation polynomial.

Recall that the size of the mesh depends on the order of the interpolation polynomial n and the number of elements E. Assume that uniformly distributed elements are used, then two meshes with equal size can be produced if the values of n and E for these meshes are chosen according to $n_1 E_1 = n_2 E_2$. A comparison of the error norms for (53) associated with using different meshes with equal sizes is shown in Table 1. Each (n, E) combination in any one row results in different meshes with equal sizes. Therefore, the corresponding error norms in each row can be compared to evaluate—for the same mesh size—the effect of increasing n versus increasing E. Table 1 shows that for this example it is more advantageous to hold E fixed while n is increased. We stress that the above discussion is only valid for equally distributed elements. Indeed, we suspect that using an adaptive mesh where the elements are clustered near regions of sharp solution changes will improve convergence. However, adaptive meshes are outside the scope of this study and therefore we will only study equally distributed elements.

5.3 Delayed Van der Pol equation

The Van der Pol equation was introduced in the 1920s as a model to describe the oscillations in the vacuum tube triode circuit. This equation became a classical example in nonlinear dynamics and has been used widely to model systems with limit cycle oscillations. Adding a feedback term, which could be the result of a delayed feedback controller, yields a delayed Van der Pol equation according to [1, 27]

$$\ddot{x}(t) + \epsilon\left(x^2 - 1\right)x(t - \tau) + x(t) = 0. \qquad (54)$$

For $\epsilon = 0.1$ and $\tau = 4.6$, a stable periodic solution is shown in Fig. 3 with period $T \approx 6.38$ while the first derivative is shown in Fig. 4.

The results of the error analysis associated with using the spectral element method to obtain the solution are shown in Fig. 3. The reference solution shown in these figures was obtained using the spectral element method with $n = 1,000$ and $E = 1$ and it matched the solution obtained from numerical simulation. For each error norm, three curves corresponding to $E \in \{1, 2, 3\}$ are plotted as a function of n where $2 \leq n \leq 25$. For each value of E and n, an initial solution was constructed from the reference solution and then was corrected using Newton iteration. It was noticed that increasing n beyond 25 yielded 0 error norms indicating a match between the calculated solution and the reference solution.

Similar to Fig. 2, it can be seen that the method converges exponentially as evidenced by all the considered error norms. Further, the convergence rate is improved as the number of mesh points is increased via increasing E from 1 to 3. Similar conclusions can be drawn from the analysis of the derivative of the periodic solution shown in Fig. 4. Applying the stability analysis described in Sect. 4 confirmed the stability of the calculated periodic orbit.

Figure 7b shows the $\|x\|_2$ norm as a function of h, the uniform element length. The order of the interpolation polynomial was held constant at either 3, 4, or 5 while the length of the uniform elements was varied between $1/500 \leq h \leq 1$, i.e., $1 \leq E \leq 500$. It is shown that for $n = 3$, the error norm decreased linearly as h was decreased. For $n = 5$, the error norm also de-

Fig. 3 The periodic solution and the error norms for (54) (where $T \approx 6.38$). The reference solution was obtained using $n = 1{,}000$ and $E = 1$ while the error norms were calculated using (52a), (52c), and (52d). In the error plots, the values $E = 1, 2, 3$ were used whereas n was varied in the range $2 \le n \le 25$
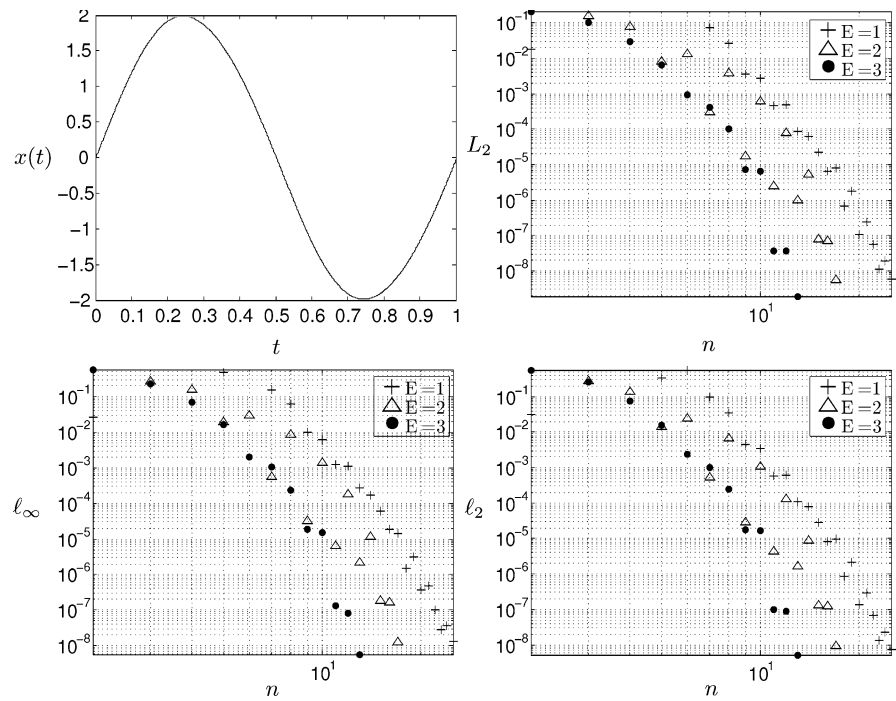
Fig. 4 The first derivative of the periodic solution to (54) and the corresponding error norms
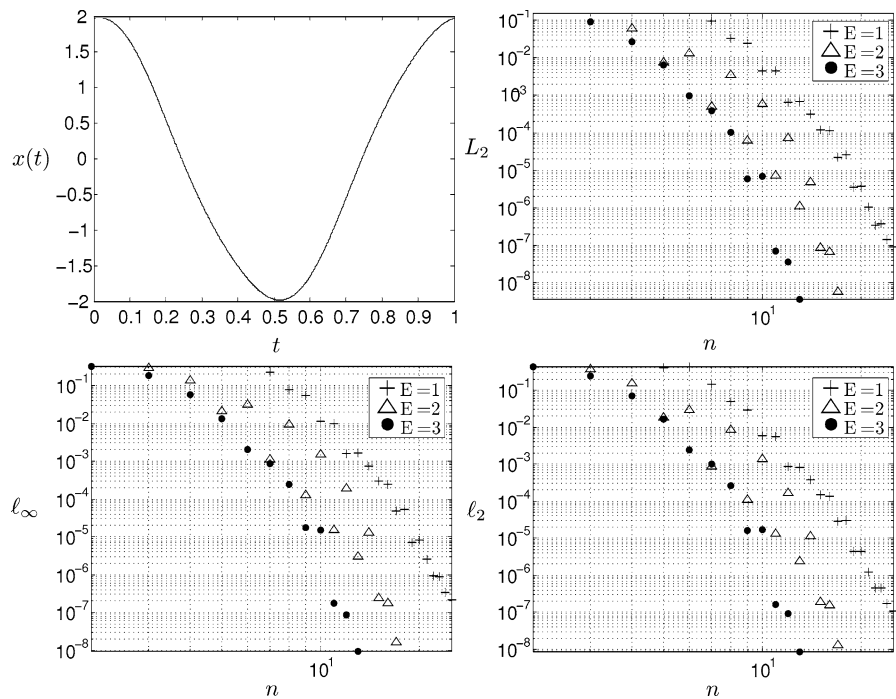
creased linearly except at $E \in \{5, 6, 7\}$ where the error dropped from $4.70e - 3$ at $E = 4$ to $4.81e - 6$ at $E = 5$ before going back up at $E = 6, 7$ to continue its linear trend. Table 4 shows the approximate rate of convergence for $n = 3$ and $n = 5$ which was found to

be approximately $O(h^n)$. However, the error plot for $n = 4$ showed a different trend. For this case, although the first part of the error plot was linear with a convergence rate of approximately $O(h^4)$ (see Table 4), it dropped from $2.67e - 5$ at $E = 16$ to $2.39e - 13$

Table 2 A comparison of the error values for (54) using different combinations of E and n that yield meshes with the same number of points

E = 1				E = 2				E = 3			
n	L_2	ℓ_2	ℓ_∞	n	L_2	ℓ_2	ℓ_∞	n	L_2	ℓ_2	ℓ_∞
x norms											
12	$4.85e-4$	$6.02e-4$	$1.10e-3$	6	$1.30e-2$	$2.38e-2$	$2.91e-2$	4	$2.93e-2$	$7.32e-2$	$6.81e-2$
18	$6.88e-7$	$8.66e-7$	$1.51e-6$	9	$1.68e-5$	$2.93e-5$	$3.27e-5$	6	$9.47e-4$	$2.40e-3$	$2.00e-3$
24	$1.91e-8$	$2.34e-8$	$3.60e-8$	12	$7.65e-5$	$1.30e-4$	$1.76e-4$	8	$9.99e-5$	$2.51e-4$	$2.29e-4$
$\dot{x}$ norms											
12	$6.57e-4$	$8.42e-4$	$1.60e-3$	6	$1.29e-2$	$2.91e-2$	$3.10e-2$	4	$2.67e-2$	$7.16e-2$	$5.74e-2$
18	$2.56e-5$	$3.05e-5$	$5.33e-5$	9	$6.25e-5$	$1.07e-4$	$1.29e-4$	6	$9.57e-4$	$2.40e-3$	$2.00e-3$
24	$1.46e-7$	$1.74e-7$	$3.35e-7$	12	$7.11e-5$	$1.69e-4$	$1.94e-4$	8	$1.03e-4$	$2.58e-4$	$2.38e-4$

at $E = 17$ where it reached a saturation region where the errors were not practically reduced as h was decreased. Similar observation can be seen for the $\|\dot{x}\|_2$ results in Fig. 7c.

A comparison of the error norms for (54) associated with using different meshes with equal sizes is shown in Table 2. Each (n, E) combination in any one row results in different meshes with equal sizes. Table 2 shows that for this example it is more advantageous to hold E fixed while n is increased. We reiterate though that the above discussion is only valid for equally distributed elements and that adaptive meshes can often yield more favorable results.

5.4 Delayed Duffing equation

The Duffing equation is another classical example of nonlinear equations. It appears in the models of many dynamical systems such as magnet-based nonlinear energy harvesters [30]. The Duffing equation was studied extensively in literature. For example, the harmonically forced delayed Duffing oscillator was investigated in [23]. However, the analysis in that study used the method of multiple scales which was confined to the case of small damping, weak nonlinearity, weak feedback and soft excitation. In the current investigation, we study the autonomous version of the delayed Duffing oscillator; however, we relax the restricting assumptions imposed in [23]. Specifically, a Duffing oscillator with state feedback can be described by the equation

$$\ddot{x}(t) + 2\zeta\dot{x}(t) + x(t) + 3\mu x^3(t)$$
$$= 2ux(t-\tau) + 2v\dot{x}(t-\tau) \tag{55}$$

where ζ, μ, u and v are scalars and $\tau > 0$ is a constant time delay. If the parameters $\zeta = \mu = u = 0.05$, $v = -0.05$ and $\tau = \pi$ are used in (55), then the resulting periodic solution (with $T \approx 4.51$) and its derivative can be described by Figs. 5 and 6, respectively.

The results of the error analysis associated with using the spectral element method to obtain the solution are also shown in these two figures. The reference solution was obtained using 500 elements each with a 5th order interpolating polynomial. For each error norm, three curves corresponding to $E \in \{1, 2, 5\}$ are plotted as a function of n where $2 \le n \le 40$. For each value of E and n, an initial solution was constructed from the reference solution and then was corrected using Newton iteration. It was noticed that the spectral element solution converged to the reference solution (zero error norms) with exponential convergence rate using the following (E, n) pairs: (1,39), (2,18), and (5,12). Faster convergence was achieved as E was increased from 1 to 5 and lower values for n were needed to obtain zero error norms. Similar conclusions can be drawn from the analysis of the derivative of the periodic solution shown in Fig. 6. Applying the stability analysis described in Sect. 4 confirmed the stability of the calculated periodic orbit.

Figure 7d shows the $\|x\|_2$ norm as a function of h—the uniform element length. The order of the interpolation polynomial was held constant at either 3, 4 or 5 while the length of the uniform elements was varied between $1/500 \le h \le 1$, i.e., $1 \le E \le 500$. It is shown that for $n = 3$, the error norm decreased linearly as h was decreased. For $n = 5$, the error norm also decreased linearly except at one point. Specifically, the

Fig. 5 The periodic solution and the error norms for (55) (where $T \approx 4.51$). The reference solution was obtained using $E = 500$ and $n = 1,000$ while the error norms were calculated using (52a), (52c), and (52d). In the error plots, the values $E = 1, 2, 5$ were used whereas n was varied in the range $2 \leq n \leq 40$
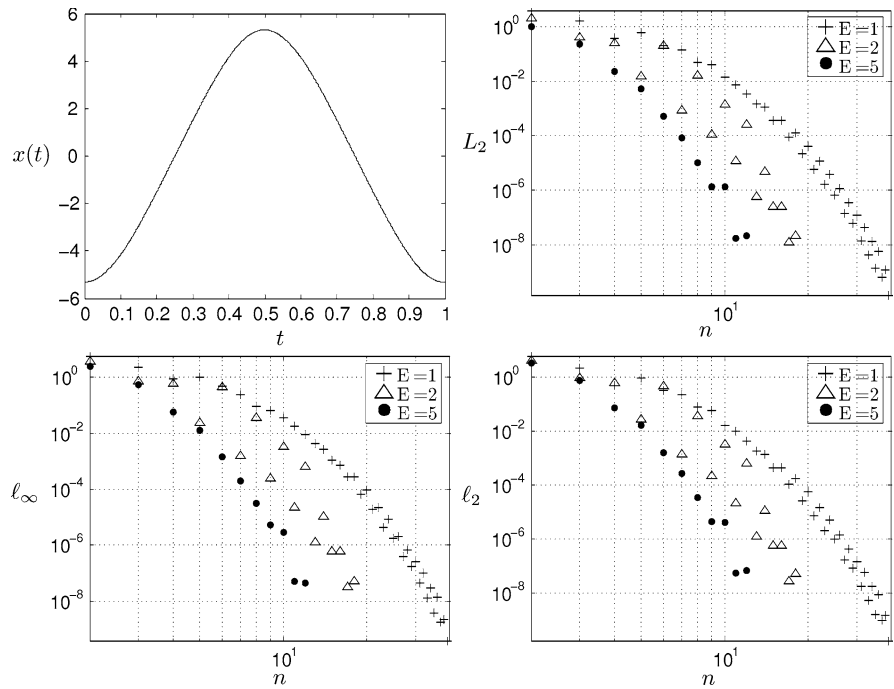
Fig. 6 The first derivative of the periodic solution to (55) and the corresponding error norms
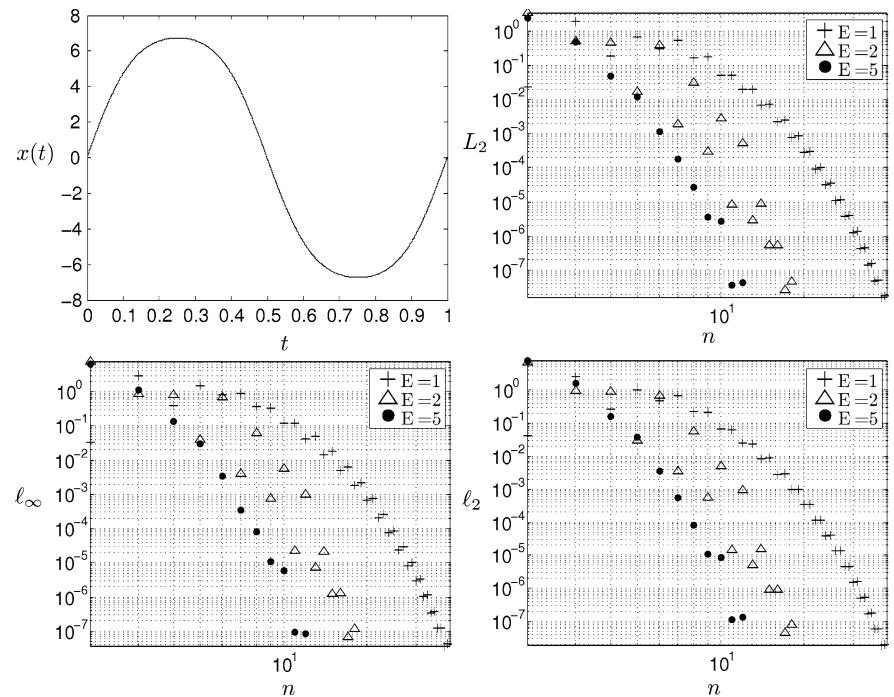
error dropped from $6.87e-4$ at $E = 7$ to $1.42e-13$ at $E = 8$ before going back to $2.37e-4$ at $E = 9$ and continuing the initial linear trend for $E \geq 9$. Ignoring the anomaly at $E = 7$, the numerical data in Table 4

indicate that both $n = 3$ and $n = 5$ converged at a rate of approximately $O(h^n)$.

On the other hand, the case $n = 4$ showed a different behavior. For this case, the convergence rate did

Fig. 7 The L_2 error plotted against the mesh size $h = 1/E$ for (53) (**a**), (54) (**b**, **c**), and (55) (**d**, **e**) using cubic (+), quartic (∘) and quintic (×) polynomials. The *first column* shows the error of the solution whereas the *second column* shows the error of the derivative
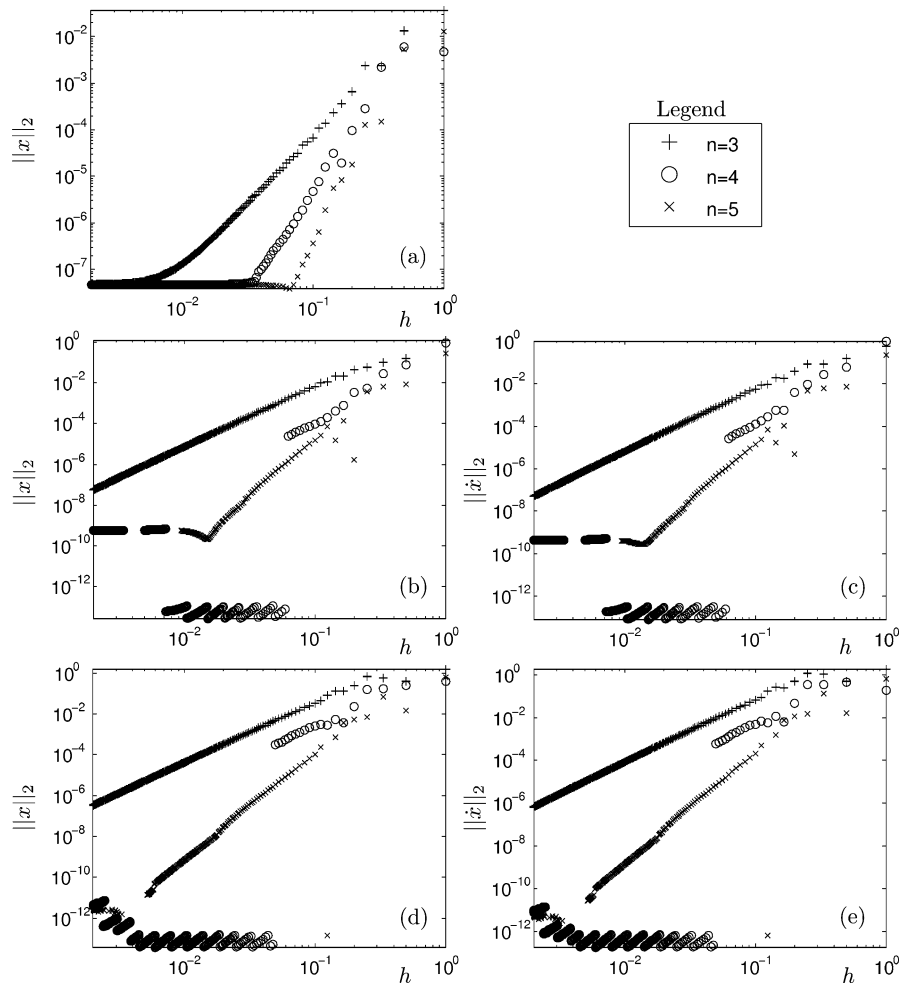
not follow a linear trend. In fact, after initially lagging behind the error for $n = 5$ case, the error for $n = 4$ dropped from $2.93e - 4$ at $E = 20$ to $5.27e - 14$ at $E = 21$ and remained in a saturation region where further decrease of h did not improve convergence. Actually, below a certain h, the errors started growing as h was decreased. This is attributed to the limitations of the double precision arithmetic that was used. To elaborate, as the errors in the solution of the spectral element method become very small, the errors in the linear solve step of the Newton iteration become relatively large [3]. Similar observation can be seen for the $\|\dot{x}\|_2$ results in Fig. 7e.

A comparison of the error norms for (55) associated with using different meshes with equal sizes is shown in Table 3. Each (n, E) combination in any one row results in different meshes with equal sizes. Table 3 shows that for this example it was more advantageous

to hold E fixed while n was increased. However, using an adaptive mesh can often yield more favorable results especially with sharply-changing solutions.

6 Conclusions

This paper considered an alternative approach to numerically approximating periodic orbits of nonlinear DDEs based on the spectral element method. This method is a modification of the spatial spectral element method which has been widely used in simulating the partial differential equations arising in models of fluids and structures [33, 41]. The temporal spectral element method can also be viewed as an evolution of the state-space temporal finite element method (state-space TFEA) which has been used to study the stability of equilibria of linear DDEs [25, 31, 38].

Table 3 A comparison of the error values for (55) using different combinations of E and n that yield meshes with the same number of points

$E = 1$				$E = 2$				$E = 3$			
n	L_2	ℓ_2	ℓ_∞	n	L_2	ℓ_2	ℓ_∞	n	L_2	ℓ_2	ℓ_∞
x norms											
20	$4.14e-5$	$5.89e-5$	$9.10e-5$	10	$1.40e-3$	$3.30e-3$	$3.30e-3$	4	$2.30e-2$	$7.60e-2$	$5.99e-2$
30	$1.20e-7$	$1.53e-7$	$2.61e-7$	15	$2.44e-7$	$5.73e-7$	$6.11e-7$	6	$5.02e-4$	$1.60e-3$	$1.50e-3$
40	0	0	0	20	0	0	0	8	$1.04e-5$	$3.44e-5$	$3.24e-5$
$\dot{x}$ norms											
20	$2.77e-4$	$3.43e-4$	$6.61e-4$	10	$2.80e-3$	$4.80e-3$	$5.60e-3$	4	$4.78e-2$	$1.52e-1$	$1.36e-1$
30	$1.26e-6$	$1.55e-6$	$2.99e-6$	15	$5.19e-7$	$9.13e-7$	$1.22e-6$	6	$1.10e-3$	$3.50e-3$	$3.50e-3$
40	0	0	0	20	0	0	0	8	$2.63e-5$	$8.34e-5$	$8.18e-5$

Table 4 Numerically computed orders of convergence for cubic, quartic and quintic polynomials with the solution of (53), the solutions and the derivative of (54), and the solution and the derivative of (55). Entries marked with a '∗' represent the order of convergence of the linear part of the error norm

	Eq. (53)	Eq. (54)		Eq. (55)	
n	$\|x\|_2$	$\|x\|_2$	$\|\dot{x}\|_2$	$\|x\|_2$	$\|\dot{x}\|_2$
3	2.78	2.95	2.94	2.91	2.90
4	4.00	3.99*	3.94*	rate not linear	rate not linear
5	5.15	5.00	5.02	5.27	5.29

The spectral element method was shown to successfully produce the periodic solutions of nonlinear DDEs. The considered case studies were obtained by introducing delays to three standard equations from the nonlinear dynamics literature: the Mackey–Glass equation (scalar), the Van der Pol equation (2nd order), and the Duffing equation (2nd order). The periodic solutions obtained with the spectral element method converged to the reference solutions as was shown in Figs. 2–6. The error norm plots showed that as n was increased, exponential rates of convergence were observed in all the considered examples.

In fact, Figs. 3–6 show that the zero error norms can be obtained for several combinations of (E, n). These figures also showed that as the size of the mesh was increased by increasing the number of elements, the solution converged faster to the reference solution. This demonstrates the *hp*-refinement capability of the current approach where 2 methods can be used to speed up convergence: either increase the number of elements E or increase the order of the interpolating polynomials n.

The L_2 error norm associated with increasing E while holding n constant was shown in Fig. 4. For the Mackey–Glass equation, it was found that the spectral element method converged at a rate of approximately $O(h^n)$ as was shown in Table 4. Similarly, for the delayed Van der Pol and the delayed Duffing equation, it was found that the error norms for 3rd and 5th order polynomials typically followed a linear trend to convergence at a rate of approximately $O(h^n)$; see Table 4. However, for the delayed Van der Pol equation, it was found that a 4th order polynomial would initially follow a linear convergence rate before reaching a critical h value where the solution would nonlinearly converge with a rate that is even faster than the 5th order polynomial rate.

Further, for the delayed Duffing equation, it was found that using a 4th order polynomial would yield nonlinear rates of convergence that would exceed those of the corresponding 5th order approximation. In addition, using a 5th order polynomial in the Duffing equation showed a linear rate of convergence except at a critical h value where the solution would seem to converge before the error increased again and continued to follow a linear trend as h was decreased. Explaining the above anomalies is a topic of future reach; however, the authors speculate that they might be associated with the accuracy of the differentiation matrix in representing the real differential operator at these n and h values.

In addition, the stability of the periodic solutions was substantiated using the concepts described in

Sect. 4. The results of this study establish the spectral element approach as a useful technique for studying nonlinear delay equations and open up a wider range of applications where this technique can be used.

References

1. Atay, F.: Van der Pol's oscillator under delayed feedback. J. Sound Vib. **218**(2), 333–339 (1998)
2. Baker, C., Bocharov, G., Ford, J., Lumb, P., Norton, S., Paul, C., Junt, T., Krebs, P., Ludewig, B.: Computational approaches to parameter estimation and model selection in immunology. J. Comput. Appl. Math. **184**(1), 50–76 (2005). doi:10.1016/j.cam.2005.02.003. Special Issue on Mathematics Applied to Immunology
3. Barton, D., Krauskopf, B., Wilson, R.: Collocation schemes for periodic solutions of neutral delay differential equations. J. Differ. Equ. Appl. **12**(11), 1087–1101 (2006). doi:10.1080/10236190601045663
4. Barton, D., Krauskopf, B., Wilson, R.: Homoclinic bifurcations in a neutral delay model of a transmission line oscillator. Nonlinearity **20**(4), 809–829 (2007). doi:10.1088/0951-7715/20/4/001
5. Bellen, A., Zennaro, M.: Numerical Solution of Delay Differential Equations. Oxford University Press, Oxford (2003)
6. Berrut, J., Trefethen, L.N.: Barycentric Lagrange interpolation. SIAM Rev. **46**(3), 501–517 (2004)
7. Bobrenkov, O., Khasawneh, F., Butcher, E., Mann, B.: Analysis of milling dynamics for simultaneously engaged cutting teeth. J. Sound Vib. **329**(5), 585–606 (2010). doi:10.1016/j.jsv.2009.09.032
8. Bocharov, G.A., Rihan, F.A.: Numerical modelling in biosciences using delay differential equations. J. Comput. Appl. Math. **125**(1-2), 183–199 (2000). doi:10.1016/S0377-0427(00)00468-4
9. Boyd, J.P.: Chebyshev and Fourier Spectral Methods. Dover, New York (2001)
10. Butcher, E., Bobrenkov, O., Bueler, E., Nindujarla, P.: Analysis of milling stability by the Chebyshev collocation method: Algorithm and optimal stable immersion levels. J. Comput. Nonlinear Dyn. **4**(3), 031003 (2009). doi:10.1115/1.3124088
11. Doedel, E., Champneys, A., Fairgrieve, T., Kuznetsov, Y., Sandstede, B., Wang, X.: Auto 97: Continuation and bifurcation software for ordinary differential equations. Available online at: http://indy.cs.concordia.ca/auto/ (1998)
12. Doedel, E.J., Keller, H.B., Kernévez, J.P.: Numerical analysis and control of bifurcation problems: II. Bifurcation in infinite dimensions. Int. J. Bifurc. Chaos **1**(4), 745–772 (1991). doi:10.1142/S0218127491000555
13. Engelborghs, K., Doedel, E.: Stability of piecewise polynomial collocation for computing periodic solutions of delay differential equations. Numer. Math. **91**, 627–648 (2002)
14. Engelborghs, K., Luzyanina, T., 'T Hout, K.J., Roose, D.: Collocation methods for the computation of periodic solutions of delay differential equations. SIAM J. Sci. Comput. **22**, 1593–1609 (2000)
15. Eslahchi, M., Masjed-Jamei, M., Babolian, E.: On numerical improvement of Gauss-Lobatto quadrature rules. Appl. Math. Comput. **164**(3), 707–717 (2005). doi:10.1016/j.amc.2004.04.113
16. Guglielmi, N., Hairer, E.: Implementing Radau IIA methods for stiff delay differential equations. Computing **67**(1), 1–12 (2001)
17. Guglielmi, N., Hairer, E.: Users' guide for the code RADAR5—version 2.1. Tech. rep., Università dell'Aquila, Italy (2005)
18. Guglielmi, N., Hairer, E.: Computing breaking points in implicit delay differential equations. Adv. Comput. Math. **29**(3), 229–247 (2008)
19. Hale, J., Sternberg, N.: Onset of chaos in differential delay equations. J. Comput. Phys. **77**(1), 221–239 (1988). doi:10.1016/0021-9991(88)90164-7
20. Hale, J.K., Lunel, S.V.: Introduction to Functional Differential Equations. Springer, New York (1993)
21. an der Heiden, U.: Unfolding complexity: hereditary dynamical systems—new bifurcation schemes and high dimensional chaos. In: Nonlinear Dynamics and Chaos: Where Do We Go From Here? IoP, Bristol (2003)
22. Higham, N.: The numerical stability of barycentric Lagrange interpolation. IMA J. Numer. Anal. **24**(4), 547–556 (2004). doi:10.1093/imanum/24.4.547
23. Hu, H., Dowell, E.H., Virgin, L.N.: Resonances of a harmonically forced duffing oscillator with time delay state feedback. Nonlinear Dyn. **15**(4), 311–327 (1998). doi:10.1023/A:1008278526811
24. Khasawneh, F., Mann, B.: A spectral element approach for the stability of delay systems. Int. J. Numer. Methods Eng. (2011). doi:10.1002/nme.3122
25. Khasawneh, F., Mann, B., Insperger, T., Stépán, G.: Increased stability of low-speed turning through a distributed force and continuous delay model. J. Comput. Nonlinear Dyn. **4**(4), 041003 (2009)
26. Krauskopf, B.: Bifurcation analysis of lasers with delay. In: Unlocking Dynamical Diversity: Optical Feedback Effects on Semiconductor Lasers, pp. 147–183, Wiley, New Jersey (2005)
27. Lin, G.: Periodic solutions for Van der Pol equation with time delay. Appl. Math. Comput. **187**(2), 1187–1198 (2007). doi:10.1016/j.amc.2006.09.032
28. Luzyanina, T., Engelborghs, K.: Computing Floquet multipliers for functional differential equations. Int. J. Bifurc. Chaos **12**(12), 2977–2989 (2002)
29. Mackey, M., Glass, L.: Oscillation and chaos in physiological control systems. Science **197**(4300), 287–289 (1977). doi:10.1126/science.267326
30. Mann, B.P., Sims, N.D.: Energy harvesting from the nonlinear oscillations of magnetic levitation. J. Sound Vib. **319**(1-2), 515–530 (2009)
31. Mann, B.P., Young, K.A.: An empirical approach for delayed oscillator stability and parametric identification. Proc. R. Soc. A **462**, 2145–2160 (2006)

32. Parter, S.: On the Legendre–Gauss–Lobatto points and weights. J. Sci. Comput. **14**(9), 347–355 (1999)

33. Patera, A.: A spectral element method for fluid dynamics: laminar flow in a channel expansion. J. Comput. Phys. **54**, 468–488 (1984)

34. Radde, N.: The impact of time delays on the robustness of biological oscillators and the effect of bifurcations on the inverse problem. EURASIP Journal on Bioinformatics and Systems. Biology **2009**, 1–14 (2009). doi:10.1155/2009/327503

35. Reddy, J.: An Introduction to the Finite Element Method, 2nd edn. McGraw-Hill, New York (1993)

36. Seydel, R.: Practical Bifurcation and Stability Analysis, 3rd edn. Springer, Berlin (2009). doi:10.1007/978-1-4419-1740-9

37. Shahverdiev, E., Bayramov, P., Shore, K.: Cascaded and adaptive chaos synchronization in multiple time-delay laser systems. Chaos Solitons Fractals **42**(1), 180–186 (2009). doi:10.1016/j.chaos.2008.11.004

38. Sims, N.D., Mann, B., Huyanan, S.: Analytical prediction of chatter stability for variable pitch and variable helix milling tools. J. Sound Vib. **317**, 664–686 (2008)

39. Stépán, G.: Retarded Dynamical Systems: Stability and Characteristic Functions. Wiley, New York (1989)

40. Szalai, R., Stépán, G.: Lobes and lenses in the stability chart of interrupted turning. J. Comput. Nonlinear Dyn. **1**, 205–211 (2006)

41. Vu, T.H., Deeks, A.J.: Use of higher-order shape functions in the scaled boundary finite element method. Int. J. Numer. Methods Eng. **65**, 1714–1733 (2006)